molecules

MDPI

Article

Design, Synthesis, Antifungal Activity, and 3D-QSAR Study of Novel Quinoxaline-2-Oxyacetate Hydrazide

Peng Teng, Yufei Li, Ruoyu Fang, Yuchuan Zhu, Peng Dai and Weihua Zhang *

Jiangsu Key Laboratory of Pesticide Science, College of Sciences, Nanjing Agricultural University, Nanjing 210095, China; tengpeng@njau.edu.cn (P.T.); 2019111022@njau.edu.cn (Y.L.); 2022811033@stu.njau.edu.cn (R.F.); 2021211010@stu.njau.edu.cn (Y.Z.); daipeng@njau.edu.cn (P.D.)
* Correspondence: zhangweihua@njau.edu.cn

Abstract: Plant pathogenic fungi pose a major threat to global food security, ecosystem services, and human livelihoods. Effective and broad-spectrum fungicides are needed to combat these pathogens. In this study, a novel antifungal 2-oxyacetate hydrazide quinoxaline scaffold as a simple analogue was designed and synthesized. Their antifungal activities were evaluated against *Botrytis cinerea* (*B. cinerea*), *Altemaria solani* (*A. solani*), *Gibberella zeae* (*G. zeae*), *Rhizoctonia solani* (*R. solani*), *Colletotrichum orbiculare* (*C. orbiculare*), and *Alternaria alternata* (*A. alternata*). These results demonstrated that most compounds exhibited remarkable inhibitory activities and possessed better efficacy than ridylbacterin, such as compound **15** (EC_{50} = 0.87 μg/mL against *G. zeae*, EC_{50} = 1.01 μg/mL against *C. orbiculare*) and compound **1** (EC_{50} = 1.54 μg/mL against *A. alternata*, EC_{50} = 0.20 μg/mL against *R. solani*). The 3D-QSAR analysis of quinoxaline-2-oxyacetate hydrazide derivatives has provided new insights into the design and optimization of novel antifungal drug molecules based on quinoxaline.

Keywords: quinoxaline; 2-oxyacetate hydrazide; antifungal activity; 3D-QSAR

check for updates

Citation: Teng, P.; Li, Y.; Fang, R.; Zhu, Y.; Dai, P.; Zhang, W. Design, Synthesis, Antifungal Activity, and 3D-QSAR Study of Novel Quinoxaline-2-Oxyacetate Hydrazide. *Molecules* **2024**, *29*, 2501. https://doi.org/10.3390/molecules29112501

Academic Editor: Alla P. Toropova

Received: 28 April 2024
Revised: 15 May 2024
Accepted: 22 May 2024
Published: 25 May 2024

Copyright: © 2024 by the authors. Licensee MDPI, Basel, Switzerland. This article is an open access article distributed under the terms and conditions of the Creative Commons Attribution (CC BY) license (https://creativecommons.org/licenses/by/4.0/).

1. Introduction

Crop pathogens pose a significant threat to food production, with fungicides serving as vital tools for disease control [1,2]. However, prolonged fungicide usage inevitably fosters increased pesticide resistance [3,4]. Therefore, the ongoing development of novel fungicides with distinctive pharmacodynamic frameworks and mechanisms of action is crucial to ensure sustainable agricultural development.

Natural products exhibit diverse structures, encompassing varied biological activities and unique mechanisms of action [5,6]. With excellent environmental compatibility, they serve as crucial sources of lead molecules for drug discovery [7,8]. Quinoxaline, a significant nitrogen-containing natural product, and its derivatives showcase a broad spectrum of biological activities [9–11], including antibacterial [12,13], antituberculosis [14], antimalarial [15], antiviral [16], anti-HIV [17], antifungal [18,19], herbicidal [20,21], and bacteriostatic [22] properties. Due to their extensive biological effects, quinoxaline derivatives hold pivotal positions in drug development research [23]. Notable examples include Glecaprevir, utilized in the treatment of chronic hepatitis C, and quinacillin, an antibiotic effective against severe bacterial infections (Figure 1).

In recent years, there has been a growing interest in the synthesis of hydrazides and their agricultural biological activities [24–30]. Compounds with a hydrazyl formate structure have demonstrated notable biological efficacy. For instance, the broad-spectrum fungicide Miexiuyihao (Figure 1) is a prominent example. Modifying the position of the oxygen element in the ester group has proven to be an effective strategy for enhancing biological activity. In 2021 [31], Chen et al. designed and synthesized quinoline 4-oxyacetate hydrazide derivatives, among which **Ac12** exhibited remarkable activity with EC_{50} values of 0.52 and 0.50 μg/mL against *S. sclerotiorum* and *B. cinerea*, surpassing the potency of both commercial fungicides azoxystrobin (both > 30.00 μg/mL) and 8-hydroxyquinoline (2.12

and 5.28 μg/mL). In this study, we focused on the design and synthesis of a novel series of quinoxolinylhydrazide derivatives. These compounds were systematically evaluated for their efficacy against six prominent crop pathogenic fungi through in vitro assays. Subsequently, the most promising compounds were chosen for a further investigation of their in vivo activity. Additionally, we sought to elucidate the primary mechanism of action using scanning electron microscopy (SEM). Furthermore, to gain deeper insights into the structure–activity relationship, a three-dimensional quantitative structure–activity relationship (3D-QSAR) model was established.

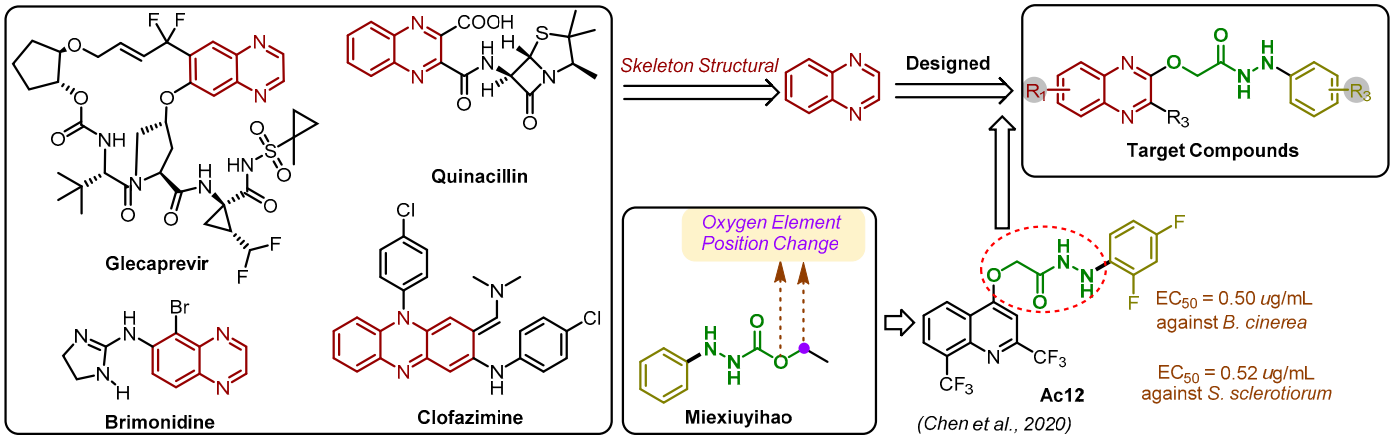

Figure 1. Design strategy of title compounds [31].

2. Results and Discussion

Chemistry. The synthetic route of the target compounds is shown in Figure 2. The structures of all compounds were identified by HRMS ^{1}H NMR and ^{13}C NMR spectroscopy (Supplementary Materials).

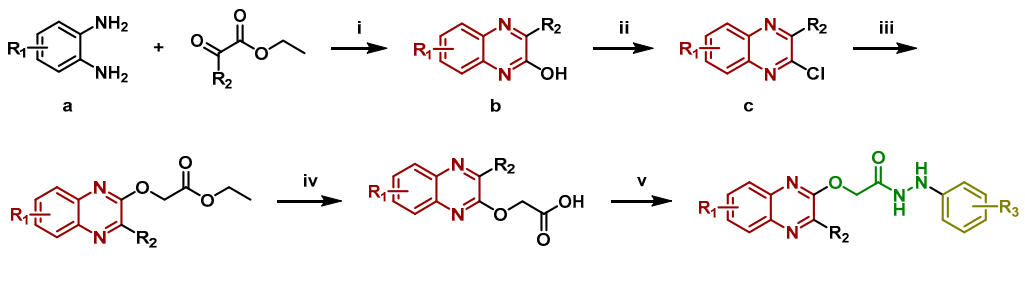

No.	R_1	R_2	R_3	No.	R_1	R_2	R_3	No.	R_1	R_2	R_3	No.	R_1	R_2	R_3
1	H	H	4-Cl	**10**	H	H	4-Ome	**19**	H	Me	2-F	**28**	6-Cl	H	4-Br
2	H	H	4-Br	**11**	H	Ph	3-F	**20**	H	Me	4-OMe	**29**	6-Cl	H	2-Br
3	H	H	3-F	**12**	H	Ph	4-CF3	**21**	6,7-Me	H	4-Cl	**30**	6-Cl	H	2-Cl
4	H	H	4-CF_3	**13**	H	Ph	4-Cl	**22**	6,7-Me	H	4-Br	**31**	6,7-Cl	H	2-Cl
5	H	H	4-Me	**14**	H	Ph	4-Br	**23**	6,7-Me	H	4-F	**32**	6,7-Cl	H	4-Cl
6	H	H	2-F	**15**	H	Me	4-CL	**24**	6,7-Me	H	2-F	**33**	6,7-Cl	H	4-Br
7	H	H	4-F	**16**	H	Me	4-F	**25**	6-Cl	H	2-F	**34**	6,7-Cl	H	3-Br
8	H	H	3-Me	**17**	H	Me	4-Br	**26**	6-Cl	H	4-F	**35**	6,7-Cl	H	2-F
9	H	H	2-Br	**18**	H	Me	4-Me	**27**	6-Cl	H	4-Cl	**36**	6,7-Cl	H	4-F

Figure 2. The synthetic route of the target compounds. Reagents and conditions. (i) H_2O, SDS; (ii) $POCl_3$, reflux; (iii) $CsCO_3$, DMSO, 80 °C, 5 h; (iv) NaOH, H_2O, rt; HCl, H_2O, rt; and (v) TBTU, Et_3N, CH_3CN. (**a**–**e**) are reaction intermediate.

In Vitro Antifungal Activity Screening. The preliminary results, presented in Table 1, illustrated the significant inhibitory activity of the target compounds against six pathogenic fungi (*B. cinerea*, *A. solani*, *G. zeae*, *R. solani*, *C. orbiculare*, and *A. alternata*) at a concentration of 20.00 μg/mL. Notably, the inhibitory activity against *B. cinerea* stood out, with compounds **6**, **20**, and **24** achieving impressive inhibitory rates exceeding 90.0%, at 97.0%, 93.8%, and 93.7%, respectively, surpassing the control drug pyrimethanil at 75.1%. While the inhibitory effect against *A. solani* was slightly lower, compound **20** still exhibited notable inhibitory activity of 94.9%. Additionally, the inhibitory effect against *G. zeae* was remarkable, with compounds **1**, **2**, **7**, **15**, **16**, **18**, **26**, and **36** displaying inhibitory rates above 90.0%, at 95.8%, 93.1%, 99.7%, 92.2%, 93.6%, 91.4%, 98.9%, and 91.2%, respectively, surpassing the control drug pyrimethanil. The most effective inhibition was observed against *R. solani*, with 24 compounds exhibiting inhibitory rates above 90.0%, including 8 compounds that completely halted its growth. Furthermore, the inhibitory activity against *C. orbiculare* was noteworthy, with 6 compounds capable of completely suppressing mycelial growth. For *A. alternata*, the inhibitory activity was outstanding, with compounds **2** and **7** exhibiting perfect inhibitory rates of 100%, and compounds **1**, **3**, **6**, **16**, **26,** and **36** demonstrating inhibitory rates above 90.0%. These findings clearly surpass those of the control drug pyrimethanil. The preliminary analysis of structure–activity relationships indicated that compounds 11 through 14 exhibited a relatively low effectiveness, with notably weaker inhibitory effects against *R. solani* compared to other substituted compounds. While some compounds retained their inhibitory capacity against *C. orbiculare*, the overall effectiveness was reduced. The activity levels were generally sustained when the quinoxaline benzene ring featured 6,7-dimethyl substitutions. In contrast, chlorine substitution on the quinoxaline benzene ring led to a decrease in overall activity, yet these compounds were more effective against *R. solani*. Notably, the activity of hydrazide compounds was significantly enhanced with halogen substitutions, but not when substituted with trifluoromethyl. This variation in activity may be attributable not only to the electronic properties of the substituents but also to their size.

Table 1. Inhibitory activities of target compounds **1**–**36** against phytopathogenic fungi [a].

Compd.	*B. cinrea*	*A. solani*	*G. zeae*	*R. solani*	*C. orbiculare*	*A. alternata*
1	86.1 ± 1.4	89.5 ± 1.2	95.8 ± 0.8	91.9 ± 0.9	100	96.4 ± 0.5
2	75.9 ± 0.5	48.1 ± 1.3	93.1 ± 0.6	94.4 ± 0.8	97.7 ± 0.5	100
3	88.8 ± 1.6	79.3 ± 0.7	59.7 ± 2.2	97.2 ± 0.7	100	91.2 ± 0.7
4	74.4 ± 1.6	66.4 ± 2.4	65.0 ± 1.2	77.4 ± 1.3	87.3 ± 1.1	85.0 ± 1.5
5	39.6 ± 3.0	40.7 ± 0.7	85.3 ± 0.6	96.4 ± 0.7	81.9 ± 0.6	60.9 ± 0.5
6	97.0 ± 0.6	80.6 ± 0	26.3 ± 0.7	70.2 ± 0.8	100	95.3 ± 2
7	80.8 ± 1.7	85.0 ± 0.7	99.7 ± 0.6	100	51.3 ± 1.0	100
8	10.2 ± 0.5	28.8 ± 1.0	<10	39.5 ± 0.8	<10	<10
9	85.6 ± 1.4	73.7 ± 1.2	29.2 ± 1.3	97.2 ± 0.7	56.2 ± 1.1	46.9 ± 0.5
10	21.9 ± 1.1	47.9 ± 0.7	31.9 ± 2.0	81.9 ± 2.1	50 ± 0.6	41.1 ± 0.7
11	14.7 ± 1.6	58.6 ± 1.0	12.8 ± 1.2	81.0 ± 0.7	83.5 ± 0.5	60.4 ± 0.7
12	52.2 ± 1.0	56.5 ± 1.9	25.6 ± 1.2	73.9 ± 2.2	50.1 ± 0.7	72.0 ± 0.6
13	56.7 ± 1.0	42.1 ± 0.7	25.8 ± 1.9	75.0 ± 0.8	35.6 ± 0.6	73.6 ± 0.8
14	28.0 ± 1.2	60.7 ± 0.7	23.9 ± 0.8	79.6 ± 1.2	34.4 ± 2.6	77.1 ± 0.7
15	80.6 ± 1.7	6.4 ± 0.7	92.2 ± 1.2	98.0 ± 0.7	91.7 ± 0.6	63.2 ± 0.7
16	70.6 ± 1.1	62.1 ± 0.7	93.6 ± 0.6	94.4 ± 0.8	95.6 ± 0.6	97.9 ± 0.7
17	74.6 ± 1.7	66.4 ± 0.7	84.7 ± 1.1	96.4 ± 0.7	60.1 ± 2.9	48.1 ± 0.7
18	81.6 ± 1.4	65.1 ± 0.8	91.4 ± 0.6	98.0 ± 1.3	94.8 ± 0.7	87.8 ± 2.4
19	20.4 ± 0.7	33.6 ± 0.7	42.2 ± 2.3	73.4 ± 0.8	18.8 ± 0.7	23.1 ± 0.7
20	93.8 ± 0.7	94.9 ± 1.4	48.1 ± 4.3	98.4 ± 0.7	100	63.8 ± 3.4
21	55.5 ± 2.0	35.0 ± 0.7	45.0 ± 1.0	73.4 ± 0.8	47.3 ± 0.5	33.1 ± 0.5
22	60.7 ± 2.4	76.4 ± 0.7	30.8 ± 0.8	97.2 ± 0.7	34.6 ± 0.6	39.6 ± 0.7
23	75.4 ± 0.7	69.1 ± 0.7	80.8 ± 1.6	97.6 ± 0.8	100	32.4 ± 0.7
24	93.7 ± 0.6	84.9 ± 1.2	25.8 ± 1.3	92.7 ± 0.7	67.2 ± 3.4	74.3 ± 0.6
25	41.5 ± 1.1	19.3 ± 0.7	15.8 ± 2.5	100	49.4 ± 0.6	50.7 ± 0.7

Table 1. *Cont.*

Compd.	*B. cinrea*	*A. solani*	*G. zeae*	*R. solani*	*C. orbiculare*	*A. alternata*
26	76.6 ± 1.1	62.1 ± 0.7	98.9 ± 0.8	100	100	91.9 ± 0.5
27	69.9 ± 2.6	46.4 ± 0.7	89.7 ± 2.2	95.2 ± 0.9	90.6 ± 0.6	56.3 ± 0.7
28	44.5 ± 2.0	39.3 ± 0.7	42.5 ± 1.6	78.0 ± 2.2	79.4 ± 0.6	45.8 ± 0.8
29	<10	20.0 ± 1.0	<10	100	14 ± 0.5	<10
30	61.7 ± 0.7	20.7 ± 0.7	33.1 ± 0.6	100	39.4 ± 0.6	54.9 ± 0.7
31	<10	23.7 ± 4.4	27.5 ± 4.4	96.8 ± 1.1	18.2 ± 1.1	22.2 ± 2.3
32	46.6 ± 1.1	54.6 ± 1.1	78.9 ± 2.6	83.9 ± 0.9	70.6 ± 1.4	60.2 ± 2.6
33	55.2 ± 3.2	53.3 ± 1.4	68.9 ± 1.9	92.5 ± 6.3	70.4 ± 1.3	48.4 ± 1.8
34	50.5 ± 1.5	70.7 ± 0.6	85.5 ± 1.1	100	65.9 ± 1.6	45.1 ± 1.4
35	14.1 ± 2.0	41.1 ± 0.8	24.8 ± 1.1	100	39.6 ± 1.7	29.3 ± 1.6
36	57.8 ± 3.3	86.1 ± 1.2	91.2 ± 0.5	100	100	92.0 ± 1.9
pyrimethanil	75.1 ± 1.0	43.1 ± 0.7	32.6 ± 1.8	89.4 ± 0.7	15.2 ± 1.1	27.2 ± 1.5

[a] Average of three replicates.

The EC_{50} values of the compounds with excellent antifungal activity were determined (Table 2). Compound **6** showed good activity against *B. cinerea*, with an EC_{50} value of 3.31 μg/mL, which was better than the control drug (3.39 μg/mL). Compound **20** exhibited better inhibitory activity against *A. solani* with an EC_{50} value of 4.42 μg/mL, superior to carbendazim (5.46 μg/mL). For *G. zeae*, 8 compounds (**1**, **2**, **7**, **15**, **16**, **18**, **26**, and **36**) demonstrated outstanding inhibitory activity; the EC_{50} values were all less than 2.00 μg/mL, significantly better than that of the control drug, ridylbacterin (2.20 μg/mL). Notably, compound **15** exhibited the highest activity, achieving an EC_{50} value of 0.87 μg/mL. For *C. orbiculare*, compounds **1**, **2**, **15**, **16**, **23**, **26**, **27**, and **36** showed the best inhibitory activity with EC_{50} values of 1.84, 1.32, 1.01, 1.35, 1.36, 1.61, 1.03, and 2.23 μg/mL, respectively, all better than carbendazim (2.32 μg/mL). Compounds **1** (EC_{50} = 1.54 μg/mL) and **7** (EC_{50} = 1.99 μg/mL) showed better inhibitory activity against *A. alternata*, better than the control drug ridylbacterin (EC_{50} = 2.07 μg/mL). For *R. solani*, 29 compounds showed excellent antifungal activity, with the EC_{50} value of target compounds being less than 1 μg/mL. Particularly, the EC_{50} value of compound **28** was 0.15 μg/mL, lower than the control drug pyrimethanil (EC_{50} = 0.21 μg/mL).

In Vivo Antifungal Activity. The inhibitory effect of compound **2** on *R. solani* in rice leaves was determined at a mass concentration of 200.00 μg/mL. As shown in Figure 3, the inhibition rate of compound **2** was 66.1% at this concentration. Compound **6**, which exhibited good activity, was selected for a tomato protection experiment, and its activity against *B. cinerea* was tested on tomato fruits at concentrations of 100.00 and 200.00 μg/mL. As depicted in Figure 3, compound **6** demonstrated significant inhibitory activity at both concentrations, with inhibition reaching 73.3% at 200.00 μg/mL. In vivo experiments demonstrated that compounds **2** and **6** retained some antifungal activity. They hold potential for further research and development.

Scanning Electron Microscopy Observations. Compound **2** was selected for scanning electron microscopy (SEM) to observe changes in the mycelium after treatment. DMSO served as the blank control. As depicted in Figure 4A–C, mycelia treated with DMSO exhibited a smooth, healthy state with a relatively uniform distribution. No folding, atrophy, or breakage of the mycelia were observed. In contrast, the mycelia of *R. solani* treated with compound **2** showed noticeable pathological changes. Figure 4D,G revealed that the mycelium of *R. solani* was disorderly distributed, intertwined, and overlapping. Some mycelia exhibited shrinkage, while Figure 4E,F,H,I showed evident pits and depressions, with some mycelia displaying distinctive protrusions that could be irregular stacks of metabolites. Overall, mycelia treated with compound **2** exhibited obvious lesions compared to those treated with DMSO, potentially affecting the direction and state of the mycelia growth by influencing the cell membrane structure of *R. solani*.

Table 2. Antifungal EC_{50} values of target compounds against phytopathogenic fungi [a].

Pathogen	Compd.	EC_{50}	Pathogen	Compd.	EC_{50}
B. Cinerea	**6**	3.31 ± 0.18	*R. solani*	**1**	0.20 ± 0.07
	20	4.36 ± 0.10		**2**	0.19 ± 0.04
	26	4.90 ± 0.05		**3**	0.58 ± 0.03
	pyrimethanil	3.39 ± 0.22		**4**	0.17 ± 0.11
A. solani	**20**	4.42 ± 0.09		**5**	0.26 ± 0.07
	carbendazim	5.46 ± 0.14		**6**	0.58 ± 0.16
G. zeae	**1**	0.94 ± 0.03		**7**	0.65 ± 0.08
	2	1.22 ± 0.06		**9**	0.84 ± 0.20
	7	1.21 ± 0.02		**10**	2.22 ± 0.06
	15	0.87 ± 0.03		**11**	1.41 ± 0.11
	16	1.17 ± 0.08		**12**	1.05 ± 0.04
	18	1.77 ± 0.04		**13**	0.20 ± 0.01
	28	1.27 ± 0.06		**14**	0.39 ± 0.08
	38	1.54 ± 0.09		**15**	0.16 ± 0.04
	pyrimethanil	2.20 ± 0.11		**16**	0.36 ± 0.12
C. orbiculare	**1**	1.84 ± 0.07		**17**	0.32 ± 0.23
	2	1.32 ± 0.06		**18**	0.52 ± 0.03
	3	3.35 ± 0.22		**19**	0.33 ± 0.11
	6	8.39 ± 0.15		**20**	0.54 ± 0.14
	15	1.01 ± 0.11		**21**	0.15 ± 0.09
	16	1.35 ± 0.07		**22**	0.47 ± 0.04
	18	3.84 ± 0.10		**23**	0.54 ± 0.14
	20	3.86 ± 0.13		**24**	0.66 ± 0.11
	23	1.36 ± 0.14		**25**	0.68 ± 0.05
	26	1.61 ± 0.12		**26**	0.55 ± 0.05
	27	1.03 ± 0.11		**27**	0.18 ± 0.04
	36	2.23 ± 0.08		**28**	0.15 ± 0.08
	carbendazim	2.32 ± 0.11		**29**	1.21 ± 0.11
A. alternata	**1**	1.54 ± 0.12		**30**	1.05 ± 0.09
	2	10.75 ± 0.05		**31**	0.80 ± 0.11
	3	7.35 ± 0.21		**32**	0.23 ± 0.05
	6	12.09 ± 0.05		**33**	0.38 ± 0.07
	7	1.99 ± 0.08		**34**	0.36 ± 0.05
	16	4.82 ± 0.25		**35**	0.55 ± 0.23
	28	2.85 ± 0.06		**36**	0.50 ± 0.15
	pyrimethanil	2.07 ± 0.15		**pyrimethanil**	0.21 ± 0.10

[a] Average of three replicates.

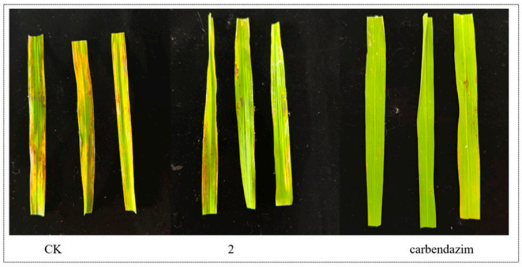

Compd.	Treatment (μg/mL)	Protection Efficary(%)
CK	-	-
2	200	66.1±3.5
Carbendazim	200	90.1±1.2

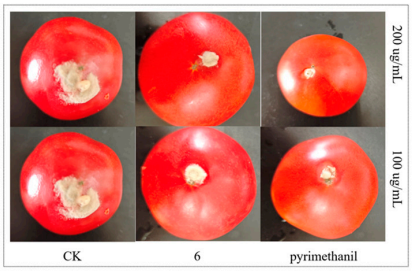

Compd.	Treatment (μg/mL)	Protection Efficary(%)
6	100	52.7±1.2
6	200	73.3±2.0
Carbendazim	200	95.6±0.7

Figure 3. The in vivo preventive effects of compound **2** against *R. solani* and compound **6** against *B. cinerea*.

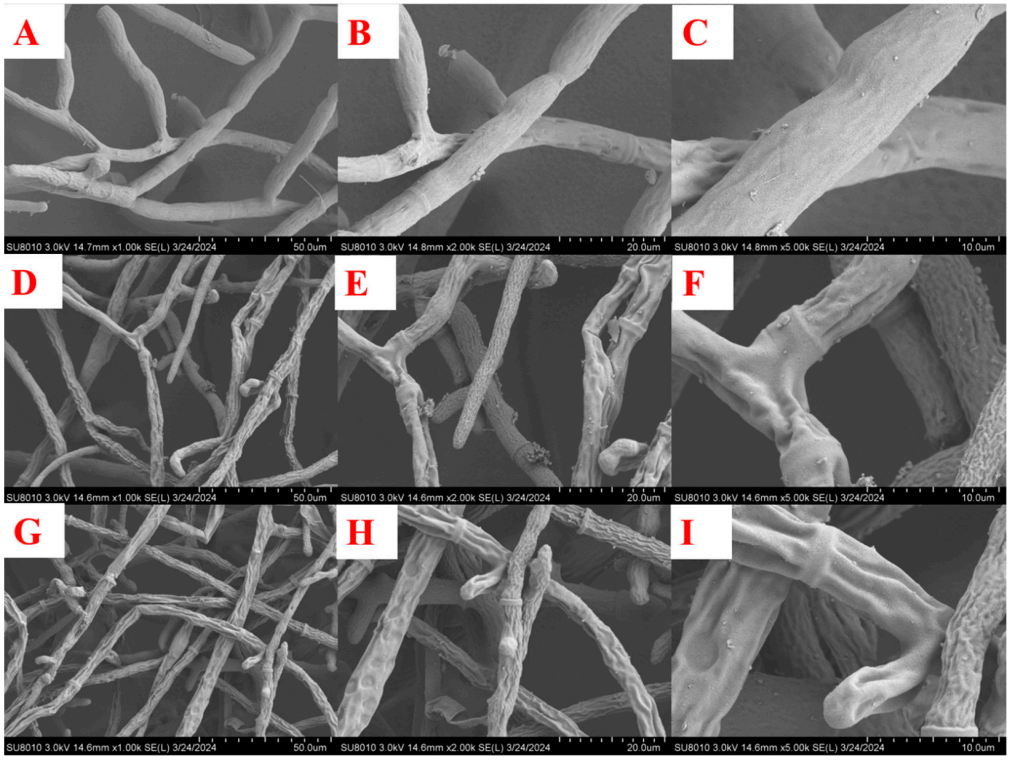

Figure 4. SEM images of *R. solani* hyphae treated by DMSO (**A**–**C**) and **2** (**D**–**I**).

Study of 3D-QSAR Models Against R. solani. To investigate the correlation between the molecular structure of quinoxolinylhydrazine derivatives and their inhibitory effectiveness against *R. solani*, effective 3D-QSAR models were developed. Then, 20 compounds (**2**–**4**, **6**, **12**, **13**, **15**–**19**, **22**, **24**, **26**, **27**, **29**–**32**, and **34**) were randomly selected to be placed in the "training set" and 10 compounds (**1**, **5**, **9**, **14**, **20**, **23**, **25**, **28**, **33**, and **25**) were selected as the "test set". These include both the comparative molecular field analysis (CoMFA) model and the comparative molecular similarity indices analysis (CoMSIA) model. Using compound **28** as the template, all compounds were superimposed. Figure 5A shows the energy-minimized structure of compound **28**, and Figure 5B displays the compound superposition diagram. Figure 6 illustrates the error and linear relationship between the pEC_{50} values predicted by the CoMFA and CoMSIA models and the experimental values.

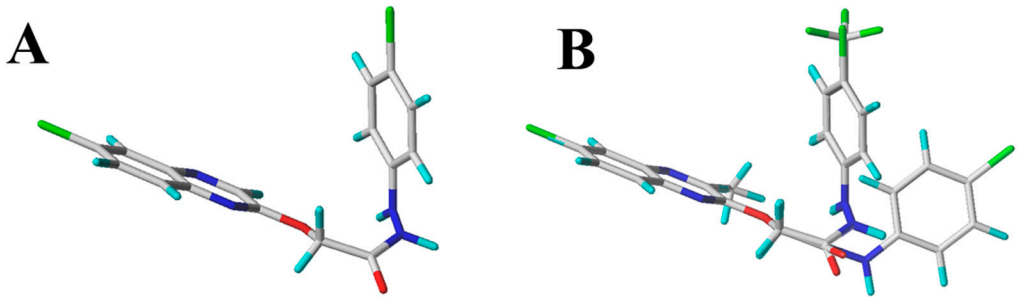

Figure 5. Template compound **28** (**A**) and composite renderings (**B**).

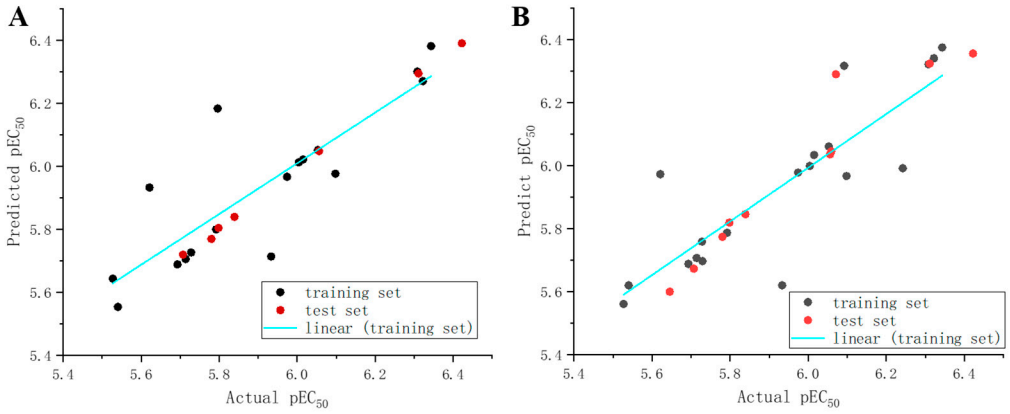

Figure 6. Experimental and predicted values of CoMFA (**A**) and CoMSIA (**B**) models pEC_{50}.

A partial least squares (PLS) analysis was conducted to establish a correlation between the chemical structures and bioactivities of the target compounds. As presented in Table 3, both the CoMFA model (with $q^2 = 0.843$ and $r^2 = 0.997$) and the CoMSIA model (with $q^2 = 0.845$ and $r^2 = 0.985$) exhibited strong robustness and internal predictive power, fulfilling the criteria of $q^2 > 0.5$ and $r^2 > 0.8$ for a reliable forecasting ability. The pEC_{50} values ($-\log EC_{50}$) were chosen as the molecular activity data for each compound. Table 4 displays the activity prediction results of the CoMFA and CoMSIA models for both the "training set" and "test set" compounds, indicating a good alignment between the predicted and experimental values, with residuals falling within an acceptable error range.

Table 3. Statistical parameters of CoMFA and CoMSIA models.

Statistical Parameter	CoMFA	CoMSIA	Validation Criteria
$q^{2\,a}$	0.843	0.845	>0.5
$r^{2\,b}$	0.997	0.985	>0.8
s ^{c}	0.025	0.038	
F ^{d}	144.141	125.981	
ONC ^{e}	14	7	

^{a} Cross-validated correlation. ^{b} Non-cross-validated correlation. ^{c} Standard error of estimate. ^{d} F-test value. ^{e} Optimum number of components.

Table 4. Actual and predicted pEC_{50} values of CoMFA and CoMSIA ^{a}.

Compd.	EC_{50}	pEC_{50}	CoMFA		CoMSIA	
			Pred pEC_{50} ^{b}	Residual	Pred pEC_{50} ^{b}	Residual
1 *	0.20 ± 0.07	6.311	6.295	0.016	6.324	−0.013
2	0.19 ± 0.04	6.343	6.382	−0.039	6.375	−0.032
3	0.58 ± 0.03	5.728	5.727	0.001	5.759	−0.031
4	0.17 ± 0.11	6.322	6.271	0.051	6.341	−0.019
5 *	0.26 ± 0.07	6.071	6.376	−0.305	6.29	−0.219
6	0.58 ± 0.16	5.729	6.193	−0.464	5.697	0.032
9 *	2.22 ± 0.06	5.645	6.209	−0.564	5.6	0.045
12	1.05 ± 0.04	5.621	5.933	−0.312	5.973	−0.352
13	0.20 ± 0.01	6.015	6.022	−0.007	6.034	−0.019
14 *	0.39 ± 0.08	6.056	6.049	0.007	6.036	0.02
15	0.12 ± 0.04	6.098	5.977	0.121	5.967	0.131
16	0.36 ± 0.12	5.974	5.967	0.007	5.978	−0.004
17	0.32 ± 0.23	6.004	6.013	−0.009	5.999	0.005
18	0.52 ± 0.03	5.792	5.800	−0.008	5.787	0.005
19	0.33 ± 0.11	6.053	6.052	0.001	6.061	−0.008
20 *	0.54 ± 0.14	5.78	5.77	0.01	5.774	0.006

Table 4. *Cont.*

Compd.	EC_{50}	pEC_{50}	CoMFA		CoMSIA	
			Pred pEC_{50} [b]	Residual	Pred pEC_{50} [b]	Residual
22	0.47 ± 0.04	5.933	5.714	0.219	5.62	0.313
23 *	0.54 ± 0.14	5.798	5.805	−0.007	5.819	−0.021
24	0.66 ± 0.11	5.714	5.706	0.008	5.707	0.007
25 *	0.68 ± 0.05	5.707	5.72	−0.013	5.673	0.034
26	0.55 ± 0.05	5.796	6.184	−0.388	6.253	−0.457
27	0.18 ± 0.04	6.308	6.301	0.007	6.322	−0.014
28 *	0.15 ± 0.08	6.422	6.391	0.031	6.356	0.066
29	1.21 ± 0.11	5.527	5.644	−0.117	5.561	−0.034
30	1.05 ± 0.09	5.540	5.554	−0.014	5.62	−0.08
31	0.80 ± 0.11	5.693	5.689	0.004	5.688	0.005
32	0.23 ± 0.05	6.242	6.048	0.194	5.992	0.25
33 *	0.38 ± 0.07	6.059	6.33	−0.271	6.045	0.014
34	0.36 ± 0.05	6.092	6.33	−0.238	6.317	−0.225
35 *	0.55 ± 0.23	5.839	5.84	−0.001	5.846	−0.007

[a] Average of three replicates. [b] $pEC_{50} = -\log(EC_{50})$; the unit of EC_{50} value needs to be converted into mol/L. * Sample of the testing set.

The following three conclusions can be drawn from the CoMFA and CoMSIA equipotential graphs shown in Figure 7. First, as depicted in Figure 7A,D, large green areas around compound **28** suggest that introducing large groups into phenylhy-drazine enhances anti-*R. solani* activity—for example, EC_{50} values **1**, **2**, **4** (R_1 = H, R_2 = H, R_3 = 4-Cl, Br, CF_3, EC_{50} = 0.20, 0.19, 0.17 μg/mL) > **7** (R_1 = H, R_2 = H, R_3 = 4-F, EC_{50} = 0.65 μg/mL), **15** (R_1 = H, R_2 = Me, R_3 = 4-Cl, EC_{50} = 0.16 μg/mL) > **16** (R_1 = H, R_2 = Me, R_3 = 4-F, EC_{50} = 0.36 μg/mL), **27**, **28** (R_1 = 6-Cl, R_2 = H, R_3 = 4-Cl, Br, EC_{50} = 0.18, 0.15 μg/mL) > **26** (R_1 = 6-Cl, R_2 = H, R_3 = 4-F, EC_{50} = 0.55 μg/mL). Second, as illustrated in Figure 7B,E, a red region at the benzene ring site of compound **28** hydrazide indicates that electron-withdrawing groups at this site improve its antifungal efficacy—for example, EC_{50} values **1**, **2**, **7** (R_1 = H, R_2 = H, R_3 = 4-Cl, Br, F, EC_{50} = 0.20, 0.19, 0.65 μg/mL) > **10** (R_1 = H, R_2 = H, R_3 = 4-OMe, EC_{50} = 2.22 μg/mL), **15**, **16**, **17** (R_1 = H, R_2 = Me, R_3 = 4-Cl, F, Br, EC_{50} = 0.16, 0.36, 0.32 μg/mL) >**18**, **20** (R_1 = H, R_2 = Me, R_3 = 4-Me, OMe, EC_{50} = 0.52, 0.54 μg/mL); according to the in vitro activity data, the inhibition rate of **8** on *R. solani* was only 39.5%, which was also consistent with the rule. Third, also shown in Figure 7B,E, red color blocks at the quinoxaline benzene ring position suggest that electron-absorbing groups here increase the antifungal activity against *R. solani*—for example, EC_{50} values **26**, **27**, **28** (R_1 = 6-Cl, R_2 = H, R_3 = 4-F, Cl, Br, EC_{50} = 0.55, 0.18, 0.15 μg/mL) > **1**, **2**, **7** (R_1 = H, R_2 = H, R_3 = 4-Cl, Br, F, EC_{50} = 0.20, 0.19, 0.65 μg/mL), **28** (R_1 = 6-Cl, R_2 = H, R_3 = 4-Br, EC_{50} = 0.15 μg/mL) > **22** (R_1 = 6,7-Me, R_2 = H, R_3 = 4-Br, EC_{50} = 0.47 μg/mL). It can be seen from the preliminary screening data of in vitro activity that **25** and **35** could completely inhibit the growth of *R. solani*, and the inhibition rate of **24** was 92.7%. Figure 7 shows that yellow, green, red, and blue color blocks are concentrated on the benzene ring, indicating that various substituents on the benzene ring significantly influence anti-*R. solani* activity. This observation aligns with the results of activity tests. Generally, the addition of electron-withdrawing groups on the benzene ring enhances anti-*R. solani* activity, particularly when F, Cl, and Br are introduced at the fourth position, significantly boosting the activity. Chlorine substitution on the quinoxaline ring also enhanced the inhibitory activity against *R. solani*, although the improvement was modest. This corresponds with the small red color block on quinoxaline in Figure 7B,E, supporting the findings from the 3D-QSAR analysis.

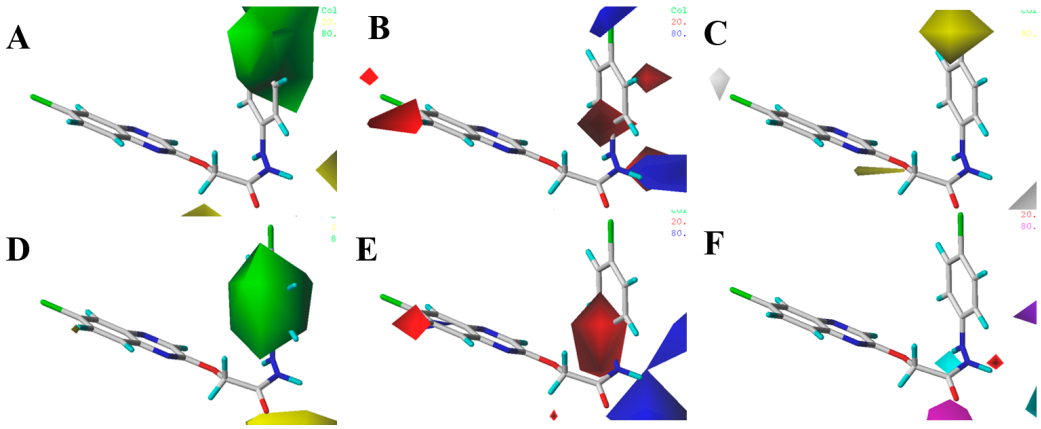

Figure 7. CoMFA (**A**,**B**) contour maps and CoMSIA (**C**–**F**) contour maps with compound **28** shown inside fields. Green and yellow modules indicate regions where steric bulk would increase and reduce anti-*R. solani* activity; blue and red modules indicate regions where electropositive and electronegative groups would increase anti-*R. solani* activity; yellow and grey modules indicate regions where hydrophobicity and hydrophilicity would increase anti-*R. solani* activity; magenta and red modules indicate regions where H-bond acceptor groups would increase and reduce the anti-*R. solani* activity, meanwhile, cyan and purple modules indicate regions where H-donor groups would increase and reduce anti-*R. solani* activity.

3. Materials and Methods

Instruments and Chemical Reagents. The reagents and solvents utilized are commercially available and do not necessitate additional purification. ^{1}H NMR and ^{13}C NMR were measured by a BRUKER-400 NMR instrument (Bruker Corporation, Rheinstetten, Germany) with $CDCl_3$, or DMSO-d_6 as the solvent and tetramethylsilane (TMS) as the internal standard. High-resolution mass spectra (HRMS) data were collected with a Triple TOF 5600 plus LCMS spectrometer (AB Sciex, Framingham, MA, USA). The melting points (mp) were determined using the Buchi M-560 Melting Point Apparatus (BUCHI, Flawil, Switzerland).

General Method of Synthesis. The synthetic route of the compounds is shown in the Figure 2. The synthesis methods of intermediates *b* and *c* refer to the reported methods [18,32].

General Synthesis method for the Intermediate d. Intermediate *c* (5.00 mmol) and Caesium Carbonate (20.00 mmol) were added to 20.00 mL DMSO. We added ethyl glycolate (7.50 mmol) slowly. The reaction was stirred at 80 °C. The reaction was monitored using thin-layer chromatography (TLC) until the reaction was complete. We poured the mixture into cold water and extracted it by ethyl acetate. The organic phase was dried over Na_2SO_4. Subsequently, the solvent was evaporated to yield the crude product, which underwent purification via column chromatography.

General Synthesis method for the Intermediate ***e***. Intermediate *d* (5.00 mmol) was added to 20.00 mL 1.00 M NaOH. The reaction was stirred at room temperature and monitored using TLC until the reaction was complete. Then, we adjusted the mixture to acid with 10% HCl, and white solid precipitates formed. The intermediate *e* was obtained by filtration.

General Synthesis method for Target Compounds **1**–**36**. Intermediate *e* (1.00 mmol) and 2-(1*H*-Benzotriazole-1-yl)-1,1,3,3-tetramethyluronium tetrafluoroborate (TBTU, 1.20 mmol) were added to 4.00 mL CH_3CN. Et_3N (0.50 mL) was added. The reaction was stirred at room temperature and monitored using TLC until the reaction was complete. The solvent was evaporated to yield the crude product, which underwent purification via column chromatography.

In Vitro Antifungal Activity Screening. The antifungal activity of the target compounds against six pathogenic fungi was tested by mycelium growth method [33] (more details of the target compounds for the antifungal activities test procedure are shown in the Supplementary Materials), including *B. Cinerea*, *A. Solani*, *G. zeae*, *R. solani*, *C. Orbiculare*, and *A. Alternata*. The compounds dissolved in DMSO were subsequently introduced into

a quantitative PDA (90.00 g glucose, 1000.00 g potato, 100.00 g agar, and 5.00 L water) medium to create a medicated plate, achieving a final concentration of 20.00 μg/mL. A plate was prepared with equal-volume DMSO as a blank control. All samples were incubated at 25 °C for 2–5 days, and each plate was assessed using the cross-streak method. Mean values and standard deviations (unit: cm) were computed, along with the inhibition rate following drug treatment. The calculation method is referred to as the reported method [34,35].

In Vivo Antifungal Activity. We prepared 500.00 mL of 1% Tsum 80 solution, weighed 10.00 mg of compound **2**, and dissolved it in 250.00 μL of DMSO. We used 1% Tsum 80 solution to bring the volume up to 50.00 mL, stirred well, and set it aside. In this case, the liquid concentration was 200.00 μg/mL. The blank control was prepared using 250.00 μL of DMSO and 1% Tsum 80 solution. We used the same method to prepare other required medications. In vivo antifungal activity was tested using reported methods [36–38].

Choose compounds exhibiting outstanding antifungal inhibition rates for in vitro EC_{50} determination. Five concentration gradients of 10.00, 5.00, 2.50, 1.25, and 0.625 μg/mL were established. We assess the inhibition rates of each concentration using the aforementioned method. We utilize the DPS data processing system to calculate the corresponding EC_{50} for each compound.

Scanning Electron Microscopy Observations. According to the above method, **2** plate containing drug concentration of 10.00 μg/mL was prepared, and blank control was set. *R. solani* was inoculated on the medicated plate and cultured for 36 h. The cake at the edge of the hypha was taken with a hole punch and fixed with phosphate buffer solution of glutaraldehyde. The mycelium was observed by scanning electron microscopy (Hitachi SU8010, Hitachi Co., Tokyo, Japan) with resolutions of 50.00 μm, 20.00 μm, and 10.00 μm.

Research of 3D-QSAR. Sybyl X-2.0 (Tripos, El Cerrito, CA, USA) was used to build 3D-QSAR models. The minimization of energy for the target molecular conformations was carried out utilizing the Tripos force field, along with the Gasteiger–Hückel method (with 10,000 iterations and 0.005 kcal mol-1 Å-1 convergence gradient), ensuring precision and thoroughness in the energy minimization. The characteristics of the CoMFA and CoMSIA models' fields were determined through a thorough analysis employing partial least squares (PLS) regression.

4. Conclusions

In summary, a series of quinoxolinylhydrazide derivatives were designed and synthesized. Most of the compounds exhibited notable antifungal activity, with compound **1** showing superior inhibitory effects against six pathogenic fungi. The activity against *R. solani* was particularly impressive, with 29 compounds exhibiting EC_{50} values below 1.00 μg/mL, especially compound **28**, which had an EC_{50} of 0.15 μg/mL. In vivo antifungal activity experiments confirmed that compounds **2** and **6** maintained effectiveness within living organisms. Scanning electron microscopy results suggested that compound **2** was a potential inhibitor of *R. solani*. Reliable 3D-QSAR models targeting *R. solani* were successfully developed. The results of these experiments will help identify new potential fungicides.

Supplementary Materials: The following supporting information can be downloaded at: https://www.mdpi.com/article/10.3390/molecules29112501/s1, Table S1. Antifungal EC_{50} values of target compounds against phytopathogenic fungia; Scheme S1. Keto-enol tautomerization of compound **3**.

Author Contributions: Conceptualization, P.T. and W.Z.; experiment execution and data analysis, P.T., Y.L., R.F., Y.Z. and P.D.; writing—original draft preparation, P.T.; writing—review and editing, P.T. and P.D. All authors have read and agreed to the published version of the manuscript.

Funding: This work was supported by the National Key Research and Development Program of China (2021YFD1700102).

Institutional Review Board Statement: Not applicable.

Informed Consent Statement: Not applicable.

Data Availability Statement: The data are contained within the article and Supplementary Materials.

Conflicts of Interest: The authors declare no conflicts of interest.

References

1. Li, L.; Zhu, X.-M.; Zhang, Y.-R.; Cai, Y.-Y.; Wang, J.-Y.; Liu, M.-Y.; Wang, J.-Y.; Bao, J.-D.; Lin, F.-C. Research on the Molecular Interaction Mechanism between Plants and Pathogenic Fungi. *Int. J. Mol. Sci.* **2022**, *23*, 4658. [CrossRef] [PubMed]
2. Wu, Y.-L.; Han, L.-J.; Wu, X.-M.; Jiang, W.; Liao, H.; Xu, Z.; Pan, C.-P. Trends and perspectives on general Pesticide analytical chemistry. *Adv. Agrochem.* **2022**, *1*, 113–124. [CrossRef]
3. Strange, R.N.; Scott, P.R. Plant Disease: A Threat to Global Food Security. *Annu. Rev. Phytopathol.* **2005**, *43*, 83–116. [CrossRef] [PubMed]
4. Wang, X.; Fu, X.; Chen, M.; Wang, A.; Yan, J.; Mei, Y.; Wang, M.; Yang, C. Novel 1,3,5-thiadiazine-2-thione derivatives containing a hydrazide moiety: Design, synthesis and bioactive evaluation against phytopathogenic fungi in vitro and in vivo. *Chin. Chem. Lett.* **2019**, *30*, 1419–1422. [CrossRef]
5. Swain, T. Secondary Compounds as Protective Agents. *Annu. Rev. Plant Biol.* **1977**, *28*, 479–501. [CrossRef]
6. Zhang, P.; Duan, C.-B.; Jin, B.; Ali, A.S.; Han, X.; Zhang, H.; Zhang, M.-Z.; Zhang, W.-H.; Gu, Y.-C. Recent advances in the natural products-based lead discovery for new agrochemicals. *Adv. Agrochem.* **2023**, *2*, 324–339. [CrossRef]
7. Arif, T.; Bhosale, J.D.; Kumar, N.; Mandal, T.K.; Bendre, R.S.; Lavekar, G.S.; Dabur, R. Natural products—Antifungal agents derived from plants. *J. Asian Nat. Prod. Res.* **2009**, *11*, 621–638. [CrossRef] [PubMed]
8. Roberts, D.P.; Mattoo, A.K. Sustainable Agriculture—Enhancing Environmental Benefits, Food Nutritional Quality and Building Crop Resilience to Abiotic and Biotic Stresses. *Agriculture* **2018**, *8*, 8. [CrossRef]
9. Dhameliya, T.M.; Chudasma, S.J.; Patel, T.M.; Dave, B.P. A review on synthetic account of 1,2,4-oxadiazoles as anti-infective agents. *Mol. Divers.* **2022**, *26*, 2967–2980. [CrossRef]
10. Xu, H.; Fan, L.-L. Synthesis and antifungal activities of novel 5,6-dihydro-indolo[1,2-a]quinoxaline derivatives. *Eur. J. Med. Chem.* **2011**, *46*, 1919–1925. [CrossRef]
11. Jiang, Y.; Zhu, C.-H.; Xia, Z.-H.; Zhao, H.-Q. Quinoxalinone-1,2,3-triazole derivatives as potential antifungal agents for plant anthrax disease: Design, synthesis, antifungal activity and SAR study. *Adv. Agrochem.* **2023**. [CrossRef]
12. El-Zahabi, H.S.A. Synthesis, Characterization, and Biological Evaluation of Some Novel Quinoxaline Derivatives as Antiviral Agents. *Arch. Pharm.* **2017**, *350*, 1700028–1700040. [CrossRef] [PubMed]
13. Zhao, Y.; Cheng, G.; Hao, H.; Pan, Y.; Liu, Z.; Dai, M.; Yuan, Z. In vitro antimicrobial activities of animal-used quinoxaline 1,4-di-N-oxides against mycobacteria, mycoplasma and fungi. *BMC Vet. Res.* **2016**, *12*, 186–198. [CrossRef]
14. Moreno, E.; Ancizu, S.; Pérez-Silanes, S.; Torres, E.; Aldana, I.; Monge, A. Synthesis and antimycobacterial activity of new quinoxaline-2-carboxamide 1,4-di-N-oxide derivatives. *Eur. J. Med. Chem.* **2010**, *45*, 4418–4426. [CrossRef]
15. Shekhar, A.C.; Rao, P.S.; Narsaiah, B.; Allanki, A.D.; Sijwali, P.S. Emergence of pyrido quinoxalines as new family of antimalarial agents. *Eur. J. Med. Chem.* **2014**, *77*, 280–287. [CrossRef]
16. Wilhelmsson, L.M.; Kingi, N.; Bergman, J. Interactions of Antiviral Indolo[2,3-b]quinoxaline Derivatives with DNA. *J. Med. Chem.* **2008**, *51*, 7744–7750. [CrossRef]
17. De Clercq, E. Toward Improved Anti-HIV Chemotherapy: Therapeutic Strategies for Intervention with HIV Infections. *J. Med. Chem.* **1995**, *38*, 2491–2517. [CrossRef] [PubMed]
18. Borah, B.; Chowhan, L.R. Recent advances in the transition-metal-free synthesis of quinoxalines. *RSC Adv.* **2021**, *11*, 37325–37353. [CrossRef]
19. Montana, M.; Mathias, F.; Terme, T.; Vanelle, P. Antitumoral activity of quinoxaline derivatives: A systematic review. *Eur. J. Med. Chem.* **2019**, *163*, 136–147. [CrossRef]
20. Pereira, J.A.; Pessoa, A.M.; Cordeiro, M.N.; Fernandes, R.; Prudencio, C.; Noronha, J.P.; Vieira, M. Quinoxaline, its derivatives and applications: A State of the Art review. *Eur. J. Med. Chem.* **2015**, *97*, 664–672. [CrossRef]
21. Tariq, S.; Alam, O.; Synthesis, M.A. Anti-inflammatory, p38α MAP kinase inhibitory activities and molecular docking studies of quinoxaline derivatives containing triazole moiety. *Bioorg. Chem.* **2018**, *76*, 343–358. [CrossRef] [PubMed]
22. Hu, Y.; Wang, K.; MacMillan, J.B. Hunanamycin A, an Antibiotic from a Marine-Derived Bacillus hunanensis. *Org. Lett.* **2013**, *15*, 390–393. [CrossRef] [PubMed]
23. Xia, R.; Guo, T.; He, J.; Chen, M.; Su, S.; Jiang, S.; Tang, X.; Chen, Y.; Xue, W. Antimicrobial evaluation and action mechanism of chalcone derivatives containing quinoxaline moiety. *Monatsh. Chem.* **2019**, *150*, 1325–1334. [CrossRef]
24. Chang, J.; Liu, Y.; Zhang, T.; Chen, Z.; Fang, H.; Hua, X. A Comprehensive Investigation of Hydrazide and Its Derived Structures in the Agricultural Fungicidal Field. *J. Agric. Food Chem.* **2023**, *71*, 8297–8316. [CrossRef] [PubMed]
25. Niu, J.-B.; Quan, C.-H.; Liu, Y.; Yu, G.-X.; Yang, J.-J.; Li, Y.-R.; Zhang, Y.-B.; Qi, Y.-Q.; Song, J.; Jin, C.-Y.; et al. Discovery of N-aryl sulphonamide-quinazoline derivatives as anti-gastric cancer agents in vitro and in vivo via activating the Hippo signalling pathway. *J. Enzym. Inhib. Med. Chem.* **2021**, *36*, 1715–1731. [CrossRef]
26. Sharma, P.C.; Sharma, D.; Sharma, A.; Saini, N.; Goyal, R.; Ola, M.; Chawla, R.; Thakur, V.K. Hydrazone comprising compounds as promising anti-infective agents: Chemistry and structure-property relationship. *Mater. Today Chem.* **2020**, *18*, 100349–100369. [CrossRef]

27. Stierli, D.; Eberle, M.; Lamberth, C.; Jacob, O.; Balmer, D.; Gulder, T. Quarternary α-cyanobenzylsulfonamides: A new subclass of CAA fungicides with excellent anti-Oomycetes activity. *Bioorg. Med. Chem.* **2021**, *30*, 115965. [CrossRef] [PubMed]
28. Wang, Z.-W.; Zhao, L.-X.; Ma, P.; Ye, T.; Fu, Y.; Ye, F. Fragments recombination, design, synthesis, safener activity and CoMFA model of novel substituted dichloroacetylphenyl sulfonamide derivatives. *Pest Manag. Sci.* **2021**, *77*, 1724–1738. [CrossRef] [PubMed]
29. Chen, Z.; Fang, H.; Chang, J.; Zhang, T.; Cui, Y.; Zhang, L.; Sui, J.; Ma, Q.; Su, P.; Wang, J.; et al. Natural Alkaloid Waltherione F-Derived Hydrazide Compounds Evaluated in an Agricultural Fungicidal Field. *J. Agric. Food Chem.* **2023**, *71*, 12333–12345. [CrossRef]
30. Yao, X.; Zhang, R.; Lv, B.; Wang, W.-W.; Liu, Z.; Hu, Z.; Design, D.L. Synthesis and biological evaluation of thiazole and imidazo[1,2-*a*]pyridine derivatives containing a hydrazone substructure as potential agrochemicals. *Adv. Agrochem.* **2023**, *2*, 154–162. [CrossRef]
31. Chen, Y.-J.; Ma, K.-Y.; Du, S.-S.; Zhang, Z.-J.; Wu, T.-L.; Sun, Y.; Liu, Y.-Q.; Yin, X.-D.; Zhou, R.; Yan, Y.-F.; et al. Antifungal Exploration of Quinoline Derivatives against Phytopathogenic Fungi Inspired by Quinine Alkaloids. *J. Agric. Food Chem.* **2021**, *69*, 12156–12170. [CrossRef] [PubMed]
32. Kumar, A.; Dhameliya, T.M.; Sharma, K.; Patel, K.A.; Hirani, R.V.; Bhatt, A.J. Sustainable approaches towards the synthesis of quinoxalines: An update. *J. Mol. Struct.* **2022**, *1259*, 132732–132747. [CrossRef]
33. Mao, X.; Wu, Z.; Bi, C.; Wang, J.; Zhao, F.; Gao, J.; Hou, Y.; Zhou, M. Molecular and Biochemical Characterization of Pydiflumetofen-Resistant Mutants of *Didymella bryoniae*. *J. Agric. Food Chem.* **2020**, *68*, 9120–9130. [CrossRef] [PubMed]
34. Yang, Y.D.; He, Y.H.; Ma, K.Y.; Li, H.; Zhang, Z.J.; Sun, Y.; Wang, Y.L.; Hu, G.F.; Wang, R.X.; Liu, Y.Q. Design and Discovery of Novel Antifungal Quinoline Derivatives with Acylhydrazide as a Promising Pharmacophore. *J. Agric. Food Chem.* **2021**, *69*, 8347–8357. [CrossRef] [PubMed]
35. Wang, X.; Dai, Z.C.; Chen, Y.F.; Cao, L.L.; Yan, W.; Li, S.K.; Wang, J.X.; Zhang, Z.G. Synthesis of 1,2,3-triazole hydrazide derivatives exhibiting anti-phytopathogenic activity. *Eur. J. Med. Chem.* **2017**, *126*, 171–182. [CrossRef] [PubMed]
36. Wang, X.; Wang, A.; Qiu, L.; Chen, M.; Lu, A.; Li, G.; Yang, C.; Xue, W. Expedient Discovery for Novel Antifungal Leads Targeting Succinate Dehydrogenase: Pyrazole-4-formylhydrazide Derivatives Bearing a Diphenyl Ether Fragment. *J. Agric. Food Chem.* **2020**, *68*, 14426–14437. [CrossRef]
37. Yang, C.; Sun, S.; Li, W.; Mao, Y.; Wang, Q.; Duan, Y.; Csuk, R.; Li, S. Bioactivity-Guided Subtraction of MIQOX for Easily Available Isoquinoline Hydrazides as Novel Antifungal Candidates. *J. Agric. Food Chem.* **2023**, *71*, 11341–11349. [CrossRef]
38. Zhi, X.Y.; Zhang, Y.; Li, Y.F.; Liu, Y.; Niu, W.P.; Li, Y.; Zhang, C.R.; Cao, H.; Hao, X.J.; Yang, C. Discovery of Natural Sesquiterpene Lactone 1-O-Acetylbritannilactone Analogues Bearing Oxadiazole, Triazole, or Imidazole Scaffolds for the Development of New Fungicidal Candidates. *J. Agric. Food Chem.* **2023**, *71*, 11680–11691. [CrossRef]

Disclaimer/Publisher's Note: The statements, opinions and data contained in all publications are solely those of the individual author(s) and contributor(s) and not of MDPI and/or the editor(s). MDPI and/or the editor(s) disclaim responsibility for any injury to people or property resulting from any ideas, methods, instructions or products referred to in the content.